

Magnetism and structural distortion in the $\text{La}_{0.7}\text{Sr}_{0.3}\text{MnO}_3$ metallic ferromagnet

Michael C. Martin and G. Shirane

Department of Physics, Brookhaven National Laboratory, Upton, New York 11973

Y. Endoh and K. Hirota

Department of Physics, Tohoku University, Sendai 980, Japan

Y. Moritomo and Y. Tokura

*Joint Research Center for Atom Technology, Tsukuba, Ibaraki 305, Japan
and Department of Applied Physics, University of Tokyo, Tokyo 113, Japan*

(Received 3 August 1995)

Neutron scattering studies on a single crystal of the highly correlated electron system, $\text{La}_{1-x}\text{Sr}_x\text{MnO}_3$ with $x \approx 0.3$, have been carried out elucidating both the spin and lattice dynamics of this metallic ferromagnet. We report a large measured value of the spin wave stiffness constant, which directly shows that the electron transfer energy of the d band is large. The spin dynamics, including magnetic critical scattering, demonstrate that this material behaves similar to other typical metallic ferromagnets such as Fe or Ni. The crystal structure is rhombohedral, as previously reported, for all temperatures studied (below ~ 425 K). We have observed superlattice peaks which show that the primary rhombohedral lattice distortion arises from oxygen octahedra rotations resulting in an $R\bar{3}c$ structure. The superlattice reflection intensities, which are very sensitive to structural changes, are independent of temperature demonstrating that there is no primary lattice distortion anomaly at the magnetic transition temperature $T_C = 378.1$ K; however, there is a lattice contraction. [S0163-1829(96)04121-5]

INTRODUCTION

The correlation between magnetism and conductivity in $\text{La}_{1-x}\text{Sr}_x\text{MnO}_3$ is a classic subject extensively studied during the 1950s and 60s.¹⁻⁴ Undoped ($x=0$), LaMnO_3 is an antiferromagnetic insulator. Upon doping with Sr, this perovskite oxide becomes a ferromagnetic metal; the change of magnetism was well explained by the double exchange hopping mechanism.⁵⁻⁸ Since the discovery of the high temperature superconducting copper oxides, study of these hole-doped manganese oxides has seen a revival. This renewed interest is due partly to the fact that LaMnO_3 is a charge gap insulator⁹ associated with the large correlation energy of the d electrons in the e_g band, and also to the discovery of giant magnetoresistance phenomena in samples with Sr dopant densities in the $0.2 \leq x \leq 0.4$ regime.¹⁰⁻¹³ The structural phase transition can also be induced by magnetic fields when the doping level is near $x \approx 0.17$.¹⁴

In LaMnO_3 , the four $3d$ electrons on the Mn site (Mn^{3+}) share both the lower t_{2g} band and the higher e_g band ($3d^4: t_{2g}^3 e_g^1$). Due to a strong Hund coupling, all the spins are parallel on a given Mn site. The electrons in the e_g band are highly correlated, creating the large correlation gap above the Fermi energy. Sr dopants naturally induce holes in the e_g band near the Fermi energy, eventually producing mobile holes and conduction. At some hole doping level the ordering changes from antiferromagnetic to ferromagnetic with a large effective magnetic moment since the intra-atomic Hund coupling is strong enough¹⁵ to align the spins within the same ionic site. Due to the strong intra-atomic ferromagnetic coupling between the itinerant holes and the localized spins ($S=3/2$), the spins first cant (tilt) until the

system becomes a ferromagnet upon doping with holes. The current understanding of the Sr-doped systems is similar to the double exchange mechanism,⁵⁻⁸ but also includes a highly correlated electron system's metal-insulator transition¹⁶ or a strong electron-phonon interaction,¹⁷ which relate back to the high- T_C copper oxide materials.

Tokura and co-workers recently observed a giant negative change in the magnetoresistance and a substantial change in the magnetostriction near the Curie temperature (T_C) for $x \approx 0.175$ crystal.¹³ Extensive experimental studies have since been undertaken exploring a wide range of Sr doping in this manganese oxide system.^{18,19} One expects that not only the electronic parameters such as the band filling, the strength of the electron correlations and so forth, but also other dynamical properties in both spin and lattice motions (or their interplay), play a crucial role in the manifestation of the interesting bulk properties. In other words, the $\text{La}_{1-x}\text{Sr}_x\text{MnO}_3$ system provides an opportunity to study a number of important physical problems: the metal-insulator electronic transition, the antiferromagnetic-ferromagnetic ordering phase change, and the lattice dynamics in the perovskite structure associated with these phase transitions.

The spin dynamics of $\text{La}_{0.7}\text{Sr}_{0.3}\text{MnO}_3$ crystals, information crucial for determining the itineracy of the system, have not been adequately studied. In $\text{La}_{1-x}\text{Sr}_x\text{MnO}_3$ (for $x \approx 0.3$) the interatomic exchange integrals, or the ferromagnetic coupling constant between nearest neighbor manganese atom spins, is predicted to be very strong due to the large transfer energy from holes hopping in the e_g band.²⁰ This exchange constant can be directly extracted from neutron scattering measurements of the spin-wave stiffness constant.

In the present publication, we describe measurements of

the dynamical magnetic properties and show that the spin wave stiffness is large, indicating a large transferred energy and itinerant ferromagnetic behavior. In addition, we describe ongoing structural measurements which confirm that the crystal structure is rhombohedral, as previously reported;² we observe a set of superlattice reflections from which we determine this primary structural distortion is due to shifts of the oxygen atoms and it has no structural anomaly at the Curie temperature.

EXPERIMENT

The single crystal used in the present neutron scattering measurement was grown at the Joint Research Center for Atom Technology using the floating zone (FZ) method, as described in detail previously.¹⁸ The crystal size is 3–4 mm in diameter and 8 cm in length. The largest domain of the crystal, which occupies about 1/3 of its length, was lined up such that the $[1\bar{1}1]$ and $[011]$ axes lie in the scattering plane (the $[21\bar{1}]$ axis is vertical). We used the H8 and H9 triple axis spectrometers at the High Flux Beam Reactor at Brookhaven National Laboratory; H8 is a thermal (typically $E=14.7$ or 30.5 meV) neutron source, H9 provides a cold ($E=5$ meV) neutron beam. The (002) reflection of pyrolytic graphite crystals were used as monochromator and analyzer. Collimations, in sequence from reactor to detector, were $40'-40'-S-80'-80'$ for H8 and $60'-40'-30'-S-80'-80'$ for H9 for studying the magnetism. Structural investigations were carried out at these collimations, as well as using a higher resolution collimation of up to $10'-10'-S-10'-80'$ at H8.

Figure 1 shows the phase diagram for $\text{La}_{1-x}\text{Sr}_x\text{MnO}_3$. In the $0.15 \leq x \leq 0.3$ dopant regime, a phase transition from ferromagnetic insulator to ferromagnetic metal as well as from orthorhombic to rhombohedral crystal structure occurs.^{14,19} We decided to begin our investigations at higher dopant level ($x \approx 0.3$), in part due to the availability of large single crystals, and also in an effort to first understand the dynamics of a less complicated system before tackling the many interesting transitions occurring in the $0.15 \leq x \leq 0.3$ samples. At $x \approx 0.3$ the sample is a ferromagnetic metal at room temperature with a Curie temperature near 380 K. Above T_C the sample is a metallic paramagnet. The inset to Fig. 1 shows the resistivity measured on this crystal indicating that the transition from paramagnet to ferromagnet is accompanied by a large drop in the resistivity, while maintaining an overall metallic temperature dependence.

MAGNETISM

Figure 2 shows the intensity of the (011) Bragg reflection as a function of temperature. This reflection has a particularly weak nuclear structure factor, $\langle F_N \rangle^2 = 0.035 \times 10^{-24} \text{ cm}^2$, and therefore has a small intensity in the paramagnetic phase. Below T_C , magnetic scattering due to the ferromagnetism of spins aligning on the manganese atoms will produce a magnetic structure factor, $\langle F_M \rangle^2 = 2/3 (e^2 \gamma / mc^2)^2 S^2 f^2$, where the $2/3$ is because we are averaging over magnetic domains with different spin directions, the term in parentheses is a constant, $(e^2 \gamma / mc^2)^2 = 0.538$, the form factor f is known for Mn at this wave vector to be ~ 0.6 , and $S = \mu/2$ which is to be

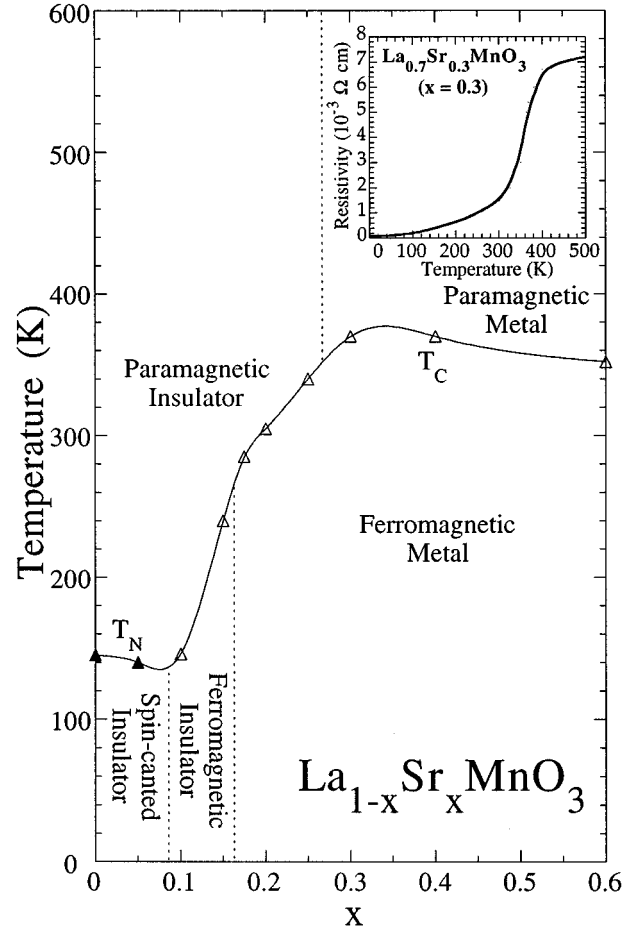


FIG. 1. Electronic and magnetic phase diagram of $\text{La}_{1-x}\text{Sr}_x\text{MnO}_3$. Inset shows resistivity of the $x=0.3$ crystal used in the present study [from Urushibara *et al.* (Ref. 19)].

determined.²² The total scattering far below T_C is given by $\langle F_N \rangle^2 + \langle F_M \rangle^2$. Using the measured peak intensities above and far below the Curie temperature from Fig. 2, we solve for a magnetic moment per Mn atom of $\mu \approx 3.6 \mu_B$. This value is close to that obtained for the similar material $\text{La}_{1-x}\text{Ca}_x\text{MnO}_3$ at $x \approx 0.3$, $\mu \approx 3.5 \mu_B$, by Wollan and Koehler² and it is close to the moment expected from adding 0.3 holes to a 4 electrons per Mn band. It is also interesting to note that this crystal of $\text{La}_{0.7}\text{Sr}_{0.3}\text{MnO}_3$ is an example of a ferromagnetic oxide with a large magnetic moment ($\mu_{\text{Mn}} \leq 4 \mu_B$) which shows metallic properties.

The inset of Fig. 2 shows the data near T_C , and a fit to a power law. The best fit gives $T_C = 378.1$ K and an exponent of $2\beta = 0.59 \pm 0.004$. The resultant exponent, $\beta = 0.295$, is below the well known three-dimensional Heisenberg ferromagnet model value of $1/3$.

We also measured the characteristics of the spin wave in the ferromagnetic state to determine how this material compares to other ferromagnets. Figure 3 plots the dispersion curve of the spin wave away from the (011) point for two temperatures ($T=300$ K $= 0.79T_C$ and $T=27$ K $= 0.07T_C$). The dispersions are well fit by parabolic functions in q ,

$$E = E_0 + Dq^2, \quad (1)$$

where E_0 is the spin wave energy gap and D is the spin wave stiffness constant. The fitted values of D (shown in Fig. 3)

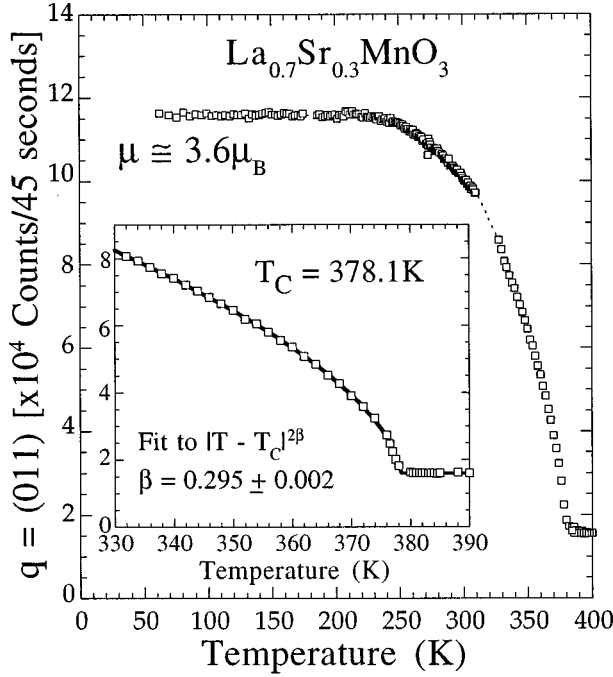


FIG. 2. Intensity of the (011) Bragg peak as a function of temperature. Inset shows the data (open squares) near the Curie temperature and a fit (solid line) to a power law. The estimated magnetic moment of the Mn ions in the ferromagnetic state is $3.6\mu_B$.

are $188 \pm 8 \text{ meV } \text{\AA}^2$ and $114 \pm 4 \text{ meV } \text{\AA}^2$ for 27 and 300 K, respectively. This change in D with temperature is very similar to previous measurements made on Fe at very low temperatures ($D=320 \text{ meV } \text{\AA}^2$) and at $0.8T_C$ ($D=175 \text{ meV } \text{\AA}^2$).²¹ Although energy scans at constant $q=(011)$ did not reveal a spin wave energy gap at either temperature within our resolution limit, the best fits to the data in Fig. 3 required small values of E_0 : $0.75 \pm 0.40 \text{ meV}$ and $0.35 \pm 0.22 \text{ meV}$ for $T=27$ and 300 K, respectively. Higher resolution experiments are needed to determine if the spin-wave energy gap is indeed nonzero.

Another important topic for study in any ferromagnetic system is the paramagnetic scattering ($T > T_C$).²¹ Constant- q scans should reveal a Lorentzian function centered at zero energy transfer with a characteristic energy width having a functional form of

$$\Gamma(q) = Af\left(\frac{\kappa_1}{q}\right)q^{2.5}, \quad (2)$$

where A is a constant,²¹ κ_1 is the inverse correlation length, and $f(\kappa_1/q)$ is the Résibois-Piette function²³ [which is unity at T_C and becomes proportional to $(\kappa_1/q)^{1/2}$ in the hydrodynamic region]. κ_1 is given by $\kappa_0 t^{0.7}$ where t the reduced temperature ($t = T/T_C$). A is related to the spin-stiffness constant D ;²⁴ when using the same system of units (meV and \AA to the appropriate power) A and D have experimentally been found to be of the same order of magnitude. In typical metallic ferromagnets such as iron and nickel, D and A are both large.²¹

We plot a constant- q scan for $\text{La}_{0.7}\text{Sr}_{0.3}\text{MnO}_3$ at $T=408 \text{ K} = 1.08T_C$ which shows a typical Lorentzian line shape in Fig. 4(a). As has been shown previously,²¹ Fig. 4(b) displays

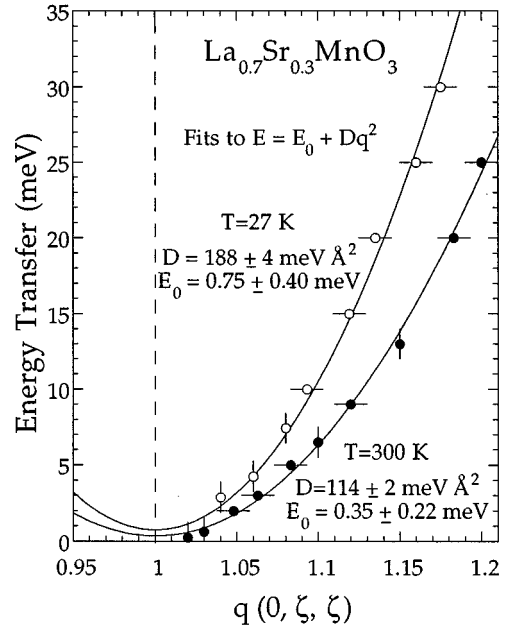


FIG. 3. Spin-wave dispersion along (011) at 300 K (solid circles) and 27 K (open circles). Horizontal lines indicate constant-energy scans; vertical lines indicate constant- q scans. Solid lines are fits to $E = E_0 + Dq^2$, where E_0 is the spin-wave energy gap and D is the spin-wave stiffness constant. The values of E_0 come from fits to the higher q data; however, no spin-wave energy gaps were directly observed at $q=0$.

a constant- E scan illustrating a profile that resembles spin waves. From these paramagnetic studies, we have made preliminary measurements of A and obtain a value of $A \sim 100 \text{ meV } \text{\AA}^{2.5}$. This value is large and indeed comparable in size to D .

STRUCTURE

Earlier measurements of $\text{La}_{0.7}\text{Sr}_{0.3}\text{MnO}_3$ (Refs. 1–4) have shown that its structure is nearly cubic, with a rhombohedral distortion. This distortion can be observed by the splitting of the (hhh) peaks along the longitudinal direction (due to different domains), as well as from an accurate alignment of the [$h00$] and [$0kk$] axes. In Fig. 5(a) we plot the high-resolution longitudinal scan through the (111) Bragg peak at room temperature. From the observed splitting we determine a value of $\alpha = 90.46 \pm 0.03^\circ$; we obtain the same α from measuring the angle between [100] and [011]. We measure the lattice constant to be $a = 3.876 \pm 0.003 \text{ \AA}$ at room temperature.

A preliminary structural study has revealed superlattice peaks at $1/2(hkl)$ [with h, k , and l all odd—one such peak is plotted in Fig. 5(b)], and missing superlattice peaks observed for $1/2(hhh)$ (with h odd). These superlattice peaks were confirmed in a powder sample study, one such 2θ scan is shown in Fig. 6. The intensities of these half-integer points, and the missing intensities of the $1/2(hhh)$ superlattice points, are well fit by a simple model for the structure factor of such points given by Axe *et al.*²⁵ for LaAlO_3 . We can therefore see that the distortion is due to rotations of the MO_6 oxygen octahedra along each (111) axis to obtain a rhombo-

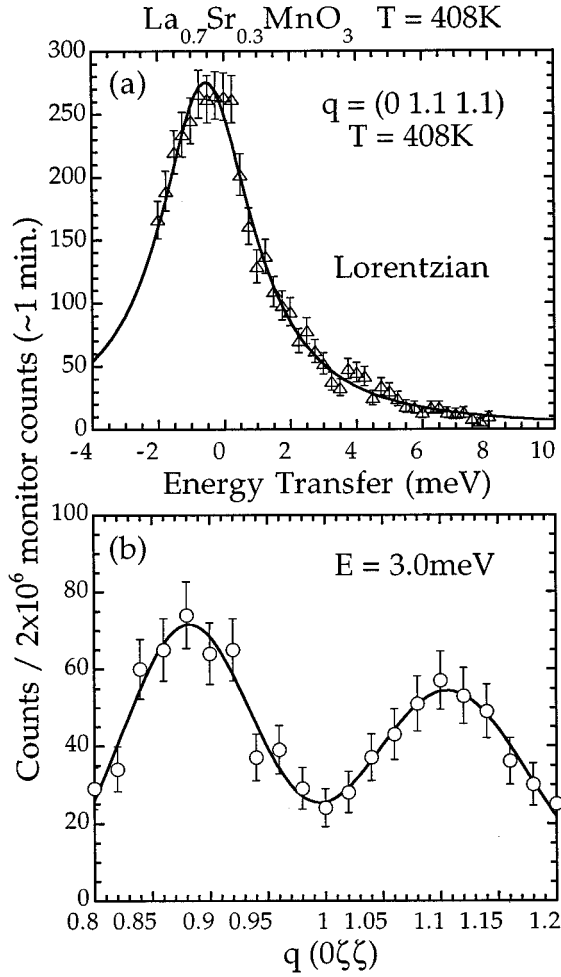


FIG. 4. A constant- q scan (a) and a constant- E scan (b) for $\text{La}_{0.7}\text{Sr}_{0.3}\text{MnO}_3$ in its paramagnetic state ($T > T_C$).

hedral symmetry or an R_{25} phonon condensation. The point group is $R\bar{3}c$, one of the most common distortions in perovskite systems,²⁶ with a rhombohedral unit cell containing two ABC_3 units.²⁷ Rietveld refinement²⁸ was carried out on the powder spectrum of Fig. 6 with the structure shown in the inset of Fig. 6. The oxygen atoms shift in the directions of the arrows by $0.24 \pm 0.01\text{ \AA}$. The Mn-O bond lengths are 1.960 \AA and the O-Mn-O angle is either 90.7° or 89.3° .

The inset to Fig. 5(b) demonstrates that the distortion indicated by these superlattice reflections is unchanged when passing through the Curie temperature [compare this to the large change due to the onset of magnetic scattering observed for the (011) Bragg peak in Fig. 2]. Rietveld fits of 300 and 400 K powder reflection data also show the oxygen shifts change by less than our measurement error bar of 0.01 \AA . Therefore this primary rhombohedral structural distortion is *not* related to the onset of ferromagnetism. If oxygen octahedra rotations are the only distortion in this material, we can rule out Jahn-Teller distortions since they freeze the rotation of the octahedra along a specific crystallographic axis at the phase transition temperature. A secondary lattice distortion, a lattice contraction of 0.1% when cooling from $T = 400\text{--}300\text{ K}$, is observed upon cooling and may or may not be related to a Jahn-Teller effect. More detailed synchrotron x-ray structural studies are in progress to determine if

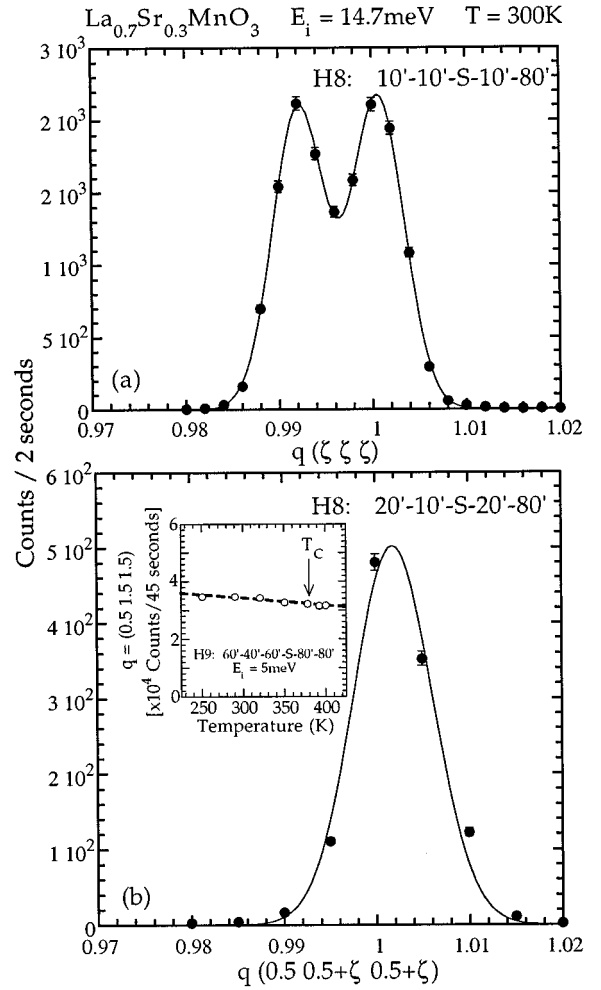


FIG. 5. (a) Splitting of the (111) peak and (b) a superlattice peak at $\frac{1}{2}(133)$ due to the rhombohedral distortion, both measured at room temperature. Inset to (b) illustrates that this structural distortion does not change when passing through T_C .

further lattice distortions are present in the $\text{La}_{0.7}\text{Sr}_{0.3}\text{MnO}_3$ system.

DISCUSSION

For localized ferromagnetic systems, the energy of the spin wave near the zone boundary is approximately equal to $k_B T_C$. However, in $\text{La}_{0.7}\text{Sr}_{0.3}\text{MnO}_3$, we find that the spin wave energy is significantly larger than the Curie temperature of 378.1 K , as demonstrated by the large value of D (the spin wave energy is on the order of a factor of three higher than T_C). Our neutron scattering measurements determining a large D (and A) therefore indicate that this system not completely localized, but instead is itinerant in character. The renormalization of T_C from the mean-field value by a Heisenberg Hamiltonian (appropriate for ferromagnetic insulators or localized spin systems) is considered to be a good measure of the itineracy; an itinerant ferromagnet will have a lower T_C compared to the mean-field value, but will have large values of A and D ,²⁹ consistent with the present results. The strong transfer energy is consistent with a moderate T_C in this itinerant system, and reflects a large J (favoring a t - J model). We have also concluded from comparing D with T_C

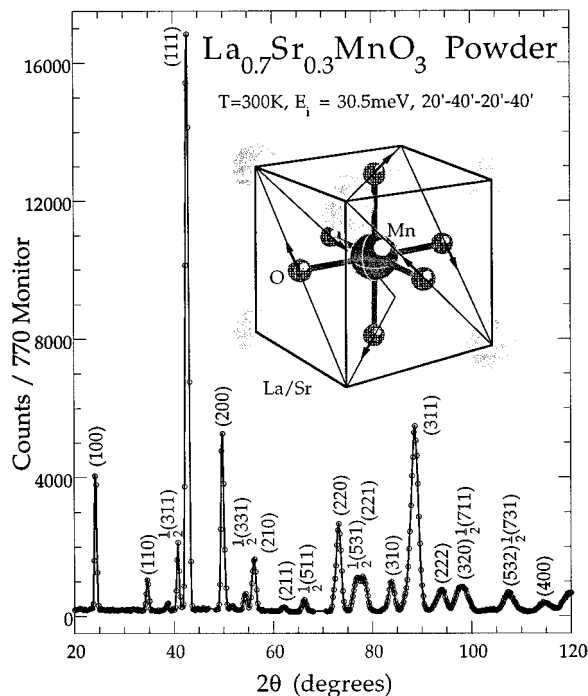


FIG. 6. Powder reflection scattering data obtained using 30.5 meV neutrons; the solid line connecting the data points is a guide to the eye and peaks are labels with the cubic indices for each reflection. The $R\bar{3}c$ structure is drawn in the inset, with arrows indicating the displacements of the oxygen atoms away from their face-centered positions.

that, even with a strong measured magnetic moment ($3.6\mu_B$), the ferromagnetism in $\text{La}_{0.7}\text{Sr}_{0.3}\text{MnO}_3$ has an itinerant character.

Evidence for polarons has been observed in the related $\text{Nd}_{0.5}\text{Pd}_{0.5}\text{MnO}_3$ compound above the Curie temperature²⁹

and polarons have been suggested as a possible explanation for the giant magnetoresistance effects observed.¹¹ A recent paper by Millis *et al.*¹⁷ argues that a polaron effect from very strong electron-phonon coupling leads to better agreement with transport results in $\text{La}_{1-x}\text{Sr}_x\text{MnO}_3$ for $0.2 \leq x \leq 0.4$. Millis *et al.* also point out that such a polaron picture requires that the fluctuating oxygen displacements should be large (of the order of 0.1 Å) for temperatures above T_C , and small for $T < T_C$. Our structural results demonstrate that the primary lattice distortion arising from R_{25} -type oxygen displacements is independent of the temperature being above or below T_C . In particular, the average oxygen atoms positions are the same within 0.01 Å at $T=400$ and 300 K. Studies are ongoing for a fluctuating oxygen position. It remains to be seen if secondary lattice distortions, such as the observed lattice contraction, are related to polarons or if we can rule out a polaron picture, at least for the $x=0.3$ compound. This still leaves the unresolved problem that double-exchange mechanisms alone do not entirely describe the properties of these materials.¹⁷

ACKNOWLEDGMENTS

We would like to thank R. J. Birgeneau, D. E. Cox, and P. Böni for enlightening discussions. This work was supported in part by the U.S.-Japan Cooperative Program on Neutron Scattering and by the Ministry of Education, Science and Culture, Japan. Research at Brookhaven National Laboratory was supported by the Division of Materials Research at the U.S. Department of Energy, under Contract No. DE-AC02-76CH00016. Work at Tohoku University was supported by the Grant-in-Aid for the Priority Area. Research at the Joint Research Center for Atom Technology was supported by the New Energy and Industrial Technology Development Organization (NEDO) of Japan.

¹G. H. Jonker and J. H. van Santen, *Physica* **16**, 337 (1950).

²E. O. Wollan and W. C. Koehler, *Phys. Rev.* **100**, 545 (1955).

³G. H. Jonker, *Physica* **22**, 707 (1956).

⁴J. B. Goodenough and J. M. Longon, in *Magnetic and Other Properties of Oxides and Related Compounds*, edited by K.-H. Hellwege and O. Madelung, Landolt-Börnstein, New Series, Group III, Vol. 4, Pt. a (Springer-Verlag, Berlin, 1970).

⁵C. Zener, *Phys. Rev.* **82**, 403 (1951).

⁶P. W. Anderson and H. Hasegawa, *Phys. Rev.* **100**, 675 (1955).

⁷P. G. deGennes, *Phys. Rev.* **100**, 564 (1955).

⁸K. Kubo and N. Ohata, *J. Phys. Soc. Jpn.* **33**, 21 (1972).

⁹T. Arima, Y. Tokura, and J. B. Torrance, *Phys. Rev. B* **48**, 17 006 (1993).

¹⁰K. Chahara, T. Ohno, M. Masahiro, and Y. Kozono, *Appl. Phys. Lett.* **63**, 1990 (1993).

¹¹R. von Helmolt, J. Wecker, B. Holzapfel, L. Schultz, and K. Samwer, *Phys. Rev. Lett.* **71**, 2331 (1993).

¹²S. Jin, T. H. Tiefel, M. McCormack, R. A. Fastnacht, R. Ramesh, and L. H. Chen, *Science* **264**, 413 (1994).

¹³Y. Tokura, A. Urushibara, Y. Moritomo, T. Arima, A. Asamitsu, G. Kido, and N. Furukawa, *J. Phys. Soc. Jpn.* **63**, 3931 (1994).

¹⁴A. Asamitsu, Y. Moritomo, Y. Tomioka, T. Arima, and Y. Tokura, *Nature* **373**, 407 (1995).

¹⁵C. Herring, in *Magnetism*, edited by J. Rado and H. Suhl (Academic, New York, 1965), Vol. 2.

¹⁶N. Furukawa, *J. Phys. Soc. Jpn.* **63**, 3214 (1994).

¹⁷A. J. Millis, P. B. Littlewood, and B. I. Shraiman, *Phys. Rev. Lett.* **74**, 5144 (1995).

¹⁸Y. Moritomo, Y. Tomioka, A. Asamitsu, Y. Tokura, and Y. Matsui, *Phys. Rev. B* **51**, 3297 (1995).

¹⁹A. Urushibara, Y. Moritomo, T. Arima, A. Asamitsu, G. Kido, and Y. Tokura, *Phys. Rev. B* **51**, 14 103 (1995).

²⁰N. Furukawa, *J. Phys. Soc. Jpn.* **63**, 3214 (1994).

²¹J. P. Wicksted, P. Böni, and G. Shirane, *Phys. Rev. B* **30**, 3655 (1984).

²²See, for example, G. E. Bacon, *Neutron Diffraction* (Oxford University Press, London, 1962), pp. 160–171.

²³R. Résibois and C. Piette, *Phys. Rev. Lett.* **24**, 514 (1970).

²⁴P. Böni, H. A. Mook, J. L. Martínez, and G. Shirane, *Phys. Rev. B* **47**, 3137 (1993).

²⁵J. D. Axe, G. Shirane, and K. A. Müller, *Phys. Rev.* **183**, 820 (1969).

²⁶A. M. Glazer, *Acta Crystallogr. B* **28**, 3384 (1972).

²⁷In the hexagonal axis scheme, $a=5.5036$ Å and $c=13.2908$ Å, with $\alpha=\beta=90^\circ$ and $\gamma=120^\circ$.

²⁸REITAN-94 computer program by F. Izumi; F. Izumi, in *The Rietveld Method*, edited by R. A. Young (Oxford University

Press, Oxford, 1993), Chap. 13; Y.-I. Kim and F. Izumi, *J. Ceram. Soc. Jpn.* **102**, 401 (1994).

²⁹G. Shirane, Y. J. Uemura, J. P. Wicksted, Y. Endoh, and Y. Ishikawa, *Phys. Rev. B* **31**, 1227 (1985).